



Multi-state lasing in self-assembled ring-shaped green fluorescent protein microcavities

Christof P. Dietrich, Sven Höfling, and Malte C. Gather

Citation: [Applied Physics Letters](#) **105**, 233702 (2014); doi: 10.1063/1.4904004

View online: <http://dx.doi.org/10.1063/1.4904004>

View Table of Contents: <http://scitation.aip.org/content/aip/journal/apl/105/23?ver=pdfcov>

Published by the [AIP Publishing](#)

Articles you may be interested in

[Polymer based planar coupling of self-assembled bottle microresonators](#)

Appl. Phys. Lett. **105**, 231114 (2014); 10.1063/1.4904013

[Nanoparticle-based protein detection by optical shift of a resonant microcavity](#)

Appl. Phys. Lett. **99**, 073701 (2011); 10.1063/1.3599706

[Ultraviolet driven negative current and rectifier effect in self-assembled green fluorescent protein device](#)

Appl. Phys. Lett. **89**, 162909 (2006); 10.1063/1.2357893

[Collective behavior and disorder-induced resonator of random lasers](#)

Appl. Phys. Lett. **86**, 171109 (2005); 10.1063/1.1920409

[Molecular-scale biophotodiode consisting of a green fluorescent protein/cytochrome c self-assembled heterolayer](#)

Appl. Phys. Lett. **84**, 2187 (2004); 10.1063/1.1655689

Not all AFMs are created equal
Asylum Research Cypher™ AFMs
There's no other AFM like Cypher

www.AsylumResearch.com/NoOtherAFMLikeIt


OXFORD
INSTRUMENTS
The Business of Science®

The advertisement features a blue background with a film strip on the left side. The text is in white and orange. The Oxford Instruments logo is in the bottom right corner.

Multi-state lasing in self-assembled ring-shaped green fluorescent protein microcavities

Christof P. Dietrich,^{a)} Sven Höfling, and Malte C. Gather^{b)}

SUPA, School of Physics and Astronomy, University of St Andrews, St Andrews KY16 9SS, United Kingdom

(Received 22 October 2014; accepted 1 December 2014; published online 10 December 2014)

We demonstrate highly efficient lasing from multiple photonic states in microcavities filled with self-assembled rings of recombinant enhanced green fluorescent protein (eGFP) in its solid state form. The lasing regime is achieved at very low excitation energies of 13 nJ and occurs from cavity modes dispersed in both energy and momentum. We attribute the momentum distribution to very efficient scattering of incident light at the surface of the eGFP rings. The distribution of lasing states in energy is induced by the large spectral width of the gain spectrum of recombinant eGFP (FWHM \cong 25 nm). © 2014 AIP Publishing LLC. [<http://dx.doi.org/10.1063/1.4904004>]

Today's laser sources meet a very wide range of different performance requirements; they reach output powers into the Peta-Watt regime,¹ achieve threshold pump energies down to a few femto-Joules,² generate pulses with atto-second durations,³ and can have total dimensions extending into the sub-wavelength scale.⁴ This is achieved by employing a vast variety of different gain materials, from gases to liquids to solid state crystals, semiconductor heterostructures, and organic molecules.

Despite increased interest in using biologically produced structures and materials for photonic applications, lasers have so far mostly relied on artificial materials. Recently, we have reported on a type of microlaser where the active component is formed by a live cell that is genetically programmed to produce a highly fluorescent protein, the so-called eGFP (enhanced green fluorescent protein).^{5,6} This work inspired further research on biologically produced gain materials in general; so far, the most notable results included the demonstration of a silk fibroin based laser,⁷ the development of microfluidic laser sensors based on fluorescent proteins,⁸ and luciferins⁹ as well as micro-droplet and distributed feedback lasers based on fluorescent flavin mononucleotides derived from the vitamin B2.^{10,11} Whilst this research impressively illustrates the broad potential of biological materials for providing optical gain, we believe that fluorescent proteins like eGFP retain a special position within the quickly growing family of biologically produced laser materials: First, nearly any organism can be genetically programmed to produce eGFP using straightforward genetic manipulation procedures, whereas many other biomaterials with attractive optical properties are restricted to certain species. Second, fluorescent proteins are characterized by a unique molecular structure, comprising of a rigid protective nano-cylinder that is 2.4 nm in diameter and 4.2 nm in height and that encloses the much smaller light emitting fluorophore at its center (Fig. 1(a)). This so-called β -barrel structure maintains a defined distance between the fluorophores of neighbouring protein molecules. We have recently found that this separation prevents concentration induced quenching of the fluorescence in fluorescent

proteins by suppressing Förster and Dexter energy transfer and thus allows the use of pure solid-state fluorescent protein as efficient optical gain material.¹² Most other biologically produced laser materials and many synthetic fluorescent dyes show nearly no fluorescence if present at high concentration or in solid state.

In this letter, we investigate the emission properties of microcavities containing self-assembled micro-rings of eGFP as active gain material. We find that the microcavities easily switch into the lasing regime at low excitation energies. The

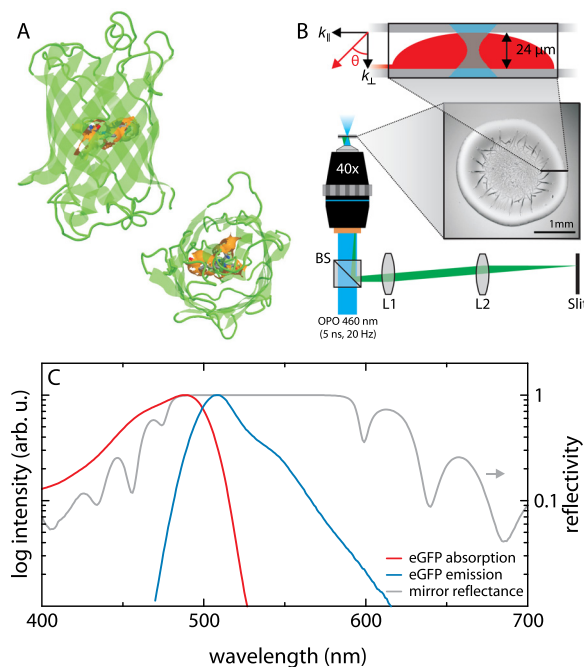


FIG. 1. (a) Schematic image (side and top view) of the eGFP fluorophore (orange) surrounded by β -sheets (green). The images are generated by using JMol 14.3.5. (b) Schematic of the experimental setup (blue: excitation beam from OPO, green: detection path of eGFP microcavity emission in Fourier imaging configuration, BS = beam splitter, L1/2 = lenses), microscopic image of the self-assembled ring-shaped eGFP microcavities; and schematic of the eGFP filled microcavity cross section with definition of the emission angle θ and the parallel and perpendicular components of the wavevector k . (c) Normalized absorption (red line) and emission spectra (blue line) of eGFP together with the reflectivity (grey line) of the dielectric mirrors forming the microcavity.

^{a)}Electronic mail: cpd3@st-andrews.ac.uk

^{b)}Electronic mail: mcg6@st-andrews.ac.uk

lasing regime is reached in several states, distributed in both momentum and energy. The momentum distribution is attributed to scattering at the surface of the eGFP rings, whereas the energy distribution between different lasing states is due to the broad gain spectrum of eGFP. Both processes lead to very efficient multi-state lasing.

Self-assembled protein rings with diameters in the millimeter range and heights of several μm were produced by pipetting $0.5\text{-}\mu\text{l}$ -droplets of a recombinant eGFP solution (45 g/l) onto a dielectric mirror and subsequently drying the material under ambient air conditions (see Fig. 1(b)).¹² In order to achieve interaction between photonic modes and the excitonic emission from eGFP, the whole structure is capped with a second (identically designed) dielectric mirror. The two distributed Bragg reflectors (DBR) above and beneath the eGFP ring consist of 13.5 pairs of alternating SiO_2 (73 nm)/ Ta_2O_5 (59 nm) layers deposited on a 1-mm thick glass substrate, creating a stop band centered at 530 nm that overlaps well with the eGFP emission band (see Fig. 1(c)). The resulting cavity thickness is about $24\ \mu\text{m}$ (see below) providing photonic modes with expected quality factors up to $Q = 5000$ (empty cavity). Photoluminescence (PL) measurements were performed with a confocal microscopic setup in epi-illumination and Fourier imaging configuration¹³ (as illustrated in Fig. 1(b)). The sample luminescence is excited by a pulsed optical parametric oscillator (OPO) system tuned to 460 nm (5 ns pulse length and 20 Hz repetition rate) being focused onto the sample surface through a $40\times$ objective ($\text{NA} = 0.55$) covering an angular range of $\pm 33^\circ$. The incident laser beam has a Gaussian profile and is focused down to a spot size of about $5\ \mu\text{m}$ (in the center of the cavity, only exciting a small fraction of the eGFP ring, see Fig. 1). The emission is then detected through the same objective and dispersed in a 500 mm spectrograph with a spectral resolution of 0.5 nm .

Angle-resolved images of the microcavity emission can be seen in Figs. 2(a)–2(c) for three different excitation laser energies of (a) 4.2 , (b) 16.7 , and (c) 420 nJ . The PL intensity is logarithmically color-coded. The image recorded at the lowest excitation energy (Fig. 1(a)) shows several, almost equidistant peaks in the spectrum whose spectral positions increase with increasing emission angle. These peaks can be assigned to emission from eGFP into modes of the cavity formed by the dielectric mirrors. The increase in mode energy

with angle is a result of their in-plane photonic dispersion ($E(k_{\parallel}) \propto \hbar k_{\parallel}^2/2m_{\text{ph}}$ and $\hbar c k_{\parallel}(\theta) = E(\theta) \sin \theta$, with m_{ph} being the photonic effective mass and θ being the emission angle, Fig. 1(b)) that becomes visible due to photonic confinement in the out-of-plane direction.¹⁴ This also highlights the direct relation between emission angle and photon momentum. Note that excitonic eGFP transitions also exhibit a dispersion relation. However, this is almost flat, i.e., the transitions have the same energy at all emission angles, due to the high effective mass of the excitons compared to cavity photons. By comparing the emission spectrum of the eGFP filled cavity at zero emission angle with the reflectivity from transfer matrix calculations (see Fig. 2 left, not accounting for any strong coupling effect), we determine a cavity thickness of $24.33\ \mu\text{m}$.¹⁵ The subsequently calculated, angle-resolved reflectivity of the eGFP microcavity is in almost perfect agreement with the experimentally obtained cavity dispersion image, confirming that the observed modes are of purely photonic nature. We therefore conclude that our microcavities operate in the weak coupling regime rather than the strong coupling regime in which the observed dispersion curves would have mixed exciton and photon character showing spectral distortions close to the individual resonances¹⁶ (even for the strong coupling regime a notable anticrossing would not be expected due to the multimodality of our system). Our calculations show that the mode numbers of the cavity modes in the chosen spectral window shown in Fig. 1 range from $m = 40$ to 48 . Note that microcavities support cavity modes with both integer and half integer mode numbers owing to the condition for constructive interference.

When increasing the excitation energy to 13 nJ/pulse , the microcavity reaches the lasing regime (see Fig. 2(b)) with a super-linear increase of the overall emission intensity (not shown here). The lasing initially starts at the bottom of the dispersion curve of cavity mode 44.5 (corresponding to a wavelength of 546 nm) and close to zero momentum (emission peak denoted as P_0 in Fig. 2(b)). The lasing wavelength coincides well with the emission spectrum of eGFP (Fig. 1(c)), confirming that the protein acts as the active gain material for the stimulated emission process (see below for further discussion). In addition, another feature of the lasing regime becomes apparent: the presence of non-zero momentum emission intensity at the wavelength of the initial lasing peak. This effect is much more pronounced at even higher

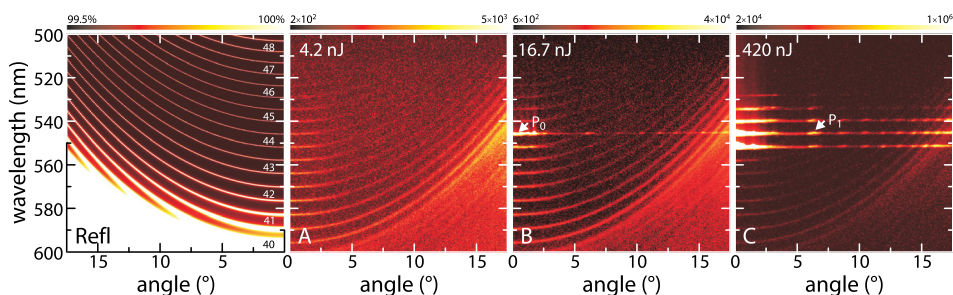


FIG. 2. Left: Calculated reflectivity of the eGFP microcavity with $d = 24.33\ \mu\text{m}$ mirror distance as a function of angle and wavelength. The corresponding integer mode numbers are given on the right hand side of the image (half integer mode number are omitted for clarity). Right: Fourier images of the eGFP microcavity emission for different excitations. The emission intensity is logarithmically color-coded (see color scales above each image). The input energies of the exciting laser beam are given in the upper left corner of each image. The images are recorded (a) well below lasing threshold, (b) in the regime of nearly exclusive zero-momentum lasing, and (c) for non-zero-momentum lasing. The white arrows indicate two lasing peaks (P_0 and P_1) with different in plane momentum.

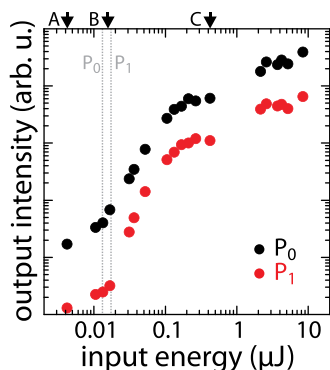


FIG. 3. Output emission intensity at 546 nm vs. input pump energy for the transitions with zero momentum (black dots, denoted P_0 in Fig. 2) and a momentum corresponding to 7° (red dots, P_1 in Fig. 2). The lasing thresholds for both cases are indicated by vertical, gray dotted lines. The arrows indicate the input energies for the Fourier images shown in Fig. 2.

excitation levels (see Fig. 2(c)) and is attributed to scattering within the cavity. The emission intensity is particularly high where the photon energy of the zero-momentum emission crosses one of the photon dispersion curves of lower order cavity modes.

To understand this behavior better, we analyzed the input-output curves for the peaks P_0 and P_1 at 546 nm (indicated in Figs. 2(b) and 2(c)). The emission intensity of peak P_0 versus laser excitation energy is shown in Fig. 3 as black dots. At low excitation, the P_0 emission increases linearly with excitation energy. The non-linear lasing regime of stimulated emission is reached at a threshold of (13.1 ± 0.5) nJ (same threshold energy as for the overall emission intensity). At an excitation of around 100 nJ, the peak intensity returns to a linear regime again, as a consequence of the fact that all available emission is now channeled into the lasing modes. The peak P_1 (red dots in Fig. 3) shows a similar behavior and also reaches the lasing regime which is unexpected given that it does not originate from the lowest possible energetic state on the dispersion curve. Its lasing threshold of (17.6 ± 1.0) nJ is slightly higher than the threshold for P_0 .

The observed features can be related to a scattering process most probably induced by the curved topography of the eGFP ring and its rough surface. This will lead to Rayleigh scattering of light from the zero-momentum state into states with finite in-plane wavevectors (i.e., finite emission angles). The scattered light is then amplified in cavity modes with suitable momentum, thus causing a series of lasing spots that are distributed in momentum but all occur at the energy of the initial zero-momentum lasing. In other words, the zero-momentum lasing serves as a “catalyst” or “seed” for the scattering induced emission at higher momentum. This interpretation is supported by two experimental observations: (i) The lasing threshold for the initial peak at zero momentum is smaller than for the finite-momentum peaks (see Figs. 3 and 4, top). (ii) The lasing threshold for all the different lasing peaks at non-zero emission angles is nearly identical (as shown in the top of Fig. 4 for the peaks at 546 nm) indicating that the lasing seeded by scattering is initiated at the same excitation conditions for all non-zero momentum peaks. Additionally, we performed similar experiments for thin films of eGFP with

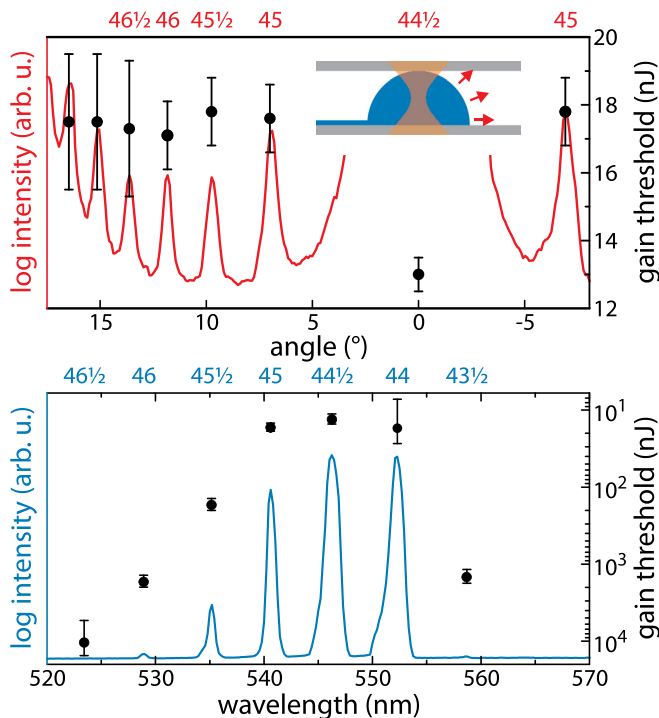


FIG. 4. Top: Angular intensity profile (recorded at 420 nJ) of high-momentum transitions at 546 nm as well as the lasing thresholds for the zero-momentum peak and the different non-zero momentum emission peaks. Bottom: Emission spectrum of the eGFP microcavity at an excitation energy of 420 nJ (integrated over all collected emission angles) and lasing thresholds for the zero-momentum emission at different wavelengths.

reduced scattering probability into higher momentum states (not shown here). Those films also showed photon lasing in the eGFP gain region but only from zero-momentum states, thus supporting our above interpretation.

Besides this scattering process into higher momentum states, Fig. 2(c) also shows that lasing is not limited to a single wavelength. In fact, several zero-momentum modes enter the regime of stimulated emission at higher excitation energies, eventually covering an extended spectral range from 520 to 560 nm. This spectral range is related to the width of the optical gain spectrum of eGFP. The lasing thresholds for the different emission wavelengths are shown in Fig. 4 bottom for all cavity modes, where lasing is accessible with our excitation conditions. For an excitation level that exactly coincides with the threshold for stimulated emission, the overall optical gain equals all losses in the system. Hence, the determined lasing threshold is a measure of the gain provided by the active material. As the cavity losses (transmission of the DBR mirrors, scattering and diffraction) are roughly constant across the spectral range over which laser emission is observed, the measured threshold values provide a qualitative measure of the gain spectrum of solid-state eGFP (spatial variations in the saturation of the gain are averaged out by the photonic wavefunction of the cavity modes owing to their high mode number). Note that the wavelength at which the lasing process initially starts and where the eGFP gain spectrum peaks (546 nm) is considerably larger than the peak wavelength of the spontaneous emission spectrum of eGFP (508 nm). This implies that there is considerable self-absorption and that strong exciton-photon coupling may be

observed in fluorescent proteins if suitably designed resonators are used.

In conclusion, we fabricated rings of eGFP in the solid state by depositing droplets of eGFP solution at ambient conditions and implemented these as active gain material in microcavity structures. This very straightforward and reproducible procedure yields eGFP microcavities that easily turn into the regime of stimulated emission with lasing threshold as small as 13 nJ. By recording the excitation-dependent, angular-resolved PL signal of the microcavities, we were able to identify several mechanisms leading to multi-state lasing from states distributed in both energy and momentum. Lasing at non-zero momentum is seeded by efficient scattering of photons in the initial zero momentum states; most probably this is caused by the morphology of the eGFP rings. The distribution of the lasing peaks in energy can be attributed to the finite width of the eGFP gain spectrum (FWHM \cong 25 nm) only allowing cavity modes inside this spectral window to enter the lasing regime. We emphasize that the observed multi-state lasing is strongly supported by the design of our microcavities and its accompanied multimodality.

We thank Kai Ostermann (TU Dresden, Germany) for providing solutions of recombinant eGFP. We acknowledge

support from the Scottish Funding Council (via SUPA) and the European Union Marie Curie Career Integration Grant (PCIG12-GA-2012-334407).

- ¹V. Yanovsky, V. Chvykov, G. Kalinchenko, P. Rousseau, T. Planchon, T. Matsuoka, and K. Krushelnick, *Opt. Express* **16**, 2109 (2008).
- ²K. Takeda, T. Sato, A. Shinya, and K. Nozaki, *Nat. Photonics* **7**, 569 (2013).
- ³P. M. Paul, E. S. Toma, P. Breger, G. Mullot, F. Audebert, P. Balcou, and P. Agostini, *Science* **292**, 1689 (2001).
- ⁴M. T. Hill and M. C. Gather, *Nat. Photonics* **8**, 908 (2014).
- ⁵M. C. Gather and S. H. Yun, *Nat. Photonics* **5**, 406 (2011).
- ⁶M. C. Gather and S. H. Yun, *Opt. Lett.* **36**, 3299 (2011).
- ⁷S. Toffanin, *Appl. Phys. Lett.* **101**, 091110 (2012).
- ⁸Q. Chen, *Lab Chip* **13**, 2679 (2013).
- ⁹X. Wu, *Appl. Phys. Lett.* **102**, 203706 (2013).
- ¹⁰S. Nizamoglu, *Adv. Mater.* **25**, 5943 (2013).
- ¹¹C. Vannahme, *Lab Chip* **13**, 2675 (2013).
- ¹²M. C. Gather and S. H. Yun, *Nat. Commun.* **5**, 5722 (2014).
- ¹³C. W. Lai, N. Y. Kim, S. Utsunomiya, G. Roumpos, H. Deng, M. D. Fraser, T. Byrnes, P. Recher, N. Kumada, T. Fujisawa, and Y. Yamamoto, *Nature* **450**, 529 (2007).
- ¹⁴A. Kavokin and G. Malpuech, *Cavity Polaritons* (Elsevier, 2003).
- ¹⁵We fitted the spectral positions of cavity modes at zero emission angle with transfer matrix simulations. The best agreement between experiment and simulation was achieved for a mirror distance of 24.33 μm .
- ¹⁶D. M. Coles and D. G. Lidzey, *Appl. Phys. Lett.* **104**, 191108 (2014).